

Charge Asymmetry of Same-Sign Dileptons in B^0 - \bar{B}^0 Mixing

E. Nakano,²⁸ K. Abe,⁷ K. Abe,³⁹ H. Aihara,⁴¹ Y. Asano,⁴⁵ T. Aushev,¹¹ A. M. Bakich,³⁶ Y. Ban,³¹ E. Barberio,¹⁹ U. Bitenc,¹² I. Bizjak,¹² S. Blyth,²⁴ A. Bondar,¹ A. Bozek,²⁵ M. Bračko,^{7, 18, 12} T. E. Browder,⁶ A. Chen,²² W. T. Chen,²² B. G. Cheon,³ Y. Choi,³⁵ A. Chuvikov,³² J. Dalseno,¹⁹ M. Danilov,¹¹ M. Dash,⁴⁶ J. Dragic,⁷ A. Drutskoy,⁴ S. Eidelman,¹ Y. Enari,²⁰ S. Fratina,¹² T. Gershon,⁷ G. Gokhroo,³⁷ B. Golob,^{17, 12} T. Hara,²⁹ N. C. Hastings,⁴¹ K. Hayasaka,²⁰ H. Hayashii,²¹ M. Hazumi,⁷ L. Hinz,¹⁶ T. Hokuue,²⁰ Y. Hoshi,³⁹ S. Hou,²² W.-S. Hou,²⁴ T. Iijima,²⁰ A. Imoto,²¹ K. Inami,²⁰ A. Ishikawa,⁷ R. Itoh,⁷ M. Iwasaki,⁴¹ J. H. Kang,⁴⁷ J. S. Kang,¹⁴ N. Katayama,⁷ H. Kawai,² T. Kawasaki,²⁷ H. R. Khan,⁴² H. Kichimi,⁷ H. O. Kim,³⁵ S. K. Kim,³⁴ S. M. Kim,³⁵ S. Korpar,^{18, 12} P. Križan,^{17, 12} P. Krokovny,¹ S. Kumar,³⁰ C. C. Kuo,²² Y.-J. Kwon,⁴⁷ J. S. Lange,⁵ G. Leder,¹⁰ T. Lesiak,²⁵ J. Li,³³ S.-W. Lin,²⁴ D. Liventsev,¹¹ G. Majumder,³⁷ D. Marlow,³² T. Matsumoto,⁴³ A. Matyja,²⁵ W. Mitaroff,¹⁰ K. Miyabayashi,²¹ H. Miyake,²⁹ H. Miyata,²⁷ R. Mizuk,¹¹ D. Mohapatra,⁴⁶ T. Mori,⁴² T. Nagamine,⁴⁰ Y. Nagasaka,⁸ M. Nakao,⁷ H. Nakazawa,⁷ Z. Natkaniec,²⁵ S. Nishida,⁷ O. Nitoh,⁴⁴ S. Ogawa,³⁸ T. Ohshima,²⁰ T. Okabe,²⁰ S. Okuno,¹³ S. L. Olsen,⁶ H. Ozaki,⁷ H. Palka,²⁵ H. Park,¹⁵ N. Parslow,³⁶ R. Pestotnik,¹² L. E. Pilonen,⁴⁶ H. Sagawa,⁷ Y. Sakai,⁷ N. Sato,²⁰ T. Schietinger,¹⁶ O. Schneider,¹⁶ M. E. Sevier,¹⁹ H. Shibuya,³⁸ V. Sidorov,¹ A. Somov,⁴ R. Stamen,⁷ S. Stanič,^{45, *} M. Starič,¹² K. Sumisawa,²⁹ S. Y. Suzuki,⁷ O. Tajima,⁷ F. Takasaki,⁷ K. Tamai,⁷ N. Tamura,²⁷ M. Tanaka,⁷ Y. Teramoto,²⁸ X. C. Tian,³¹ K. Trabelsi,⁶ T. Tsuboyama,⁷ T. Tsukamoto,⁷ S. Uehara,⁷ T. Uglov,¹¹ S. Uno,⁷ P. Urquijo,¹⁹ K. E. Varvell,³⁶ C. C. Wang,²⁴ C. H. Wang,²³ M. Watanabe,²⁷ Q. L. Xie,⁹ B. D. Yabsley,⁴⁶ A. Yamaguchi,⁴⁰ Y. Yamashita,²⁶ M. Yamauchi,⁷ J. Ying,³¹ J. Zhang,⁷ L. M. Zhang,³³ Z. P. Zhang,³³ V. Zhilich,¹ and D. Žontar^{17, 12}

(The Belle Collaboration)

¹*Budker Institute of Nuclear Physics, Novosibirsk*

²*Chiba University, Chiba*

³*Chonnam National University, Kwangju*

⁴*University of Cincinnati, Cincinnati, Ohio 45221*

⁵*University of Frankfurt, Frankfurt*

⁶*University of Hawaii, Honolulu, Hawaii 96822*

⁷*High Energy Accelerator Research Organization (KEK), Tsukuba*

⁸*Hiroshima Institute of Technology, Hiroshima*

⁹*Institute of High Energy Physics, Chinese Academy of Sciences, Beijing*

¹⁰*Institute of High Energy Physics, Vienna*

¹¹*Institute for Theoretical and Experimental Physics, Moscow*

¹²*J. Stefan Institute, Ljubljana*

¹³*Kanagawa University, Yokohama*

¹⁴*Korea University, Seoul*

- ¹⁵*Kyungpook National University, Taegu*
- ¹⁶*Swiss Federal Institute of Technology of Lausanne, EPFL, Lausanne*
- ¹⁷*University of Ljubljana, Ljubljana*
- ¹⁸*University of Maribor, Maribor*
- ¹⁹*University of Melbourne, Victoria*
- ²⁰*Nagoya University, Nagoya*
- ²¹*Nara Women's University, Nara*
- ²²*National Central University, Chung-li*
- ²³*National United University, Miao Li*
- ²⁴*Department of Physics, National Taiwan University, Taipei*
- ²⁵*H. Niewodniczanski Institute of Nuclear Physics, Krakow*
- ²⁶*Nihon Dental College, Niigata*
- ²⁷*Niigata University, Niigata*
- ²⁸*Osaka City University, Osaka*
- ²⁹*Osaka University, Osaka*
- ³⁰*Panjab University, Chandigarh*
- ³¹*Peking University, Beijing*
- ³²*Princeton University, Princeton, New Jersey 08544*
- ³³*University of Science and Technology of China, Hefei*
- ³⁴*Seoul National University, Seoul*
- ³⁵*Sungkyunkwan University, Suwon*
- ³⁶*University of Sydney, Sydney NSW*
- ³⁷*Tata Institute of Fundamental Research, Bombay*
- ³⁸*Toho University, Funabashi*
- ³⁹*Tohoku Gakuin University, Tagajo*
- ⁴⁰*Tohoku University, Sendai*
- ⁴¹*Department of Physics, University of Tokyo, Tokyo*
- ⁴²*Tokyo Institute of Technology, Tokyo*
- ⁴³*Tokyo Metropolitan University, Tokyo*
- ⁴⁴*Tokyo University of Agriculture and Technology, Tokyo*
- ⁴⁵*University of Tsukuba, Tsukuba*
- ⁴⁶*Virginia Polytechnic Institute and State University, Blacksburg, Virginia 24061*
- ⁴⁷*Yonsei University, Seoul*
- (Dated: August 19, 2019)

Abstract

We report a measurement of the charge asymmetry for same-sign dileptons in $B^0\text{-}\bar{B}^0$ mixing, A_{sl} . The data were collected with the Belle detector at KEKB. Using a data sample of 78 fb^{-1} recorded at the $\Upsilon(4S)$ resonance and 9 fb^{-1} recorded at an energy 60 MeV below the resonance, we measure $A_{\text{sl}} = (-1.1 \pm 7.9(\text{stat}) \pm 7.0(\text{sys})) \times 10^{-3}$.

PACS numbers: 11.30.Er, 12.15.Ff, 13.20.He, 14.40.Nd

*on leave from Nova Gorica Polytechnic, Nova Gorica

I. INTRODUCTION

The Standard Model allows CP violation in B^0 - \bar{B}^0 mixing [1]. In particular, there is a possible difference between the $B^0 \rightarrow \bar{B}^0$ and $\bar{B}^0 \rightarrow B^0$ transition rates that can manifest itself as a charge asymmetry in same-sign dilepton events in $\Upsilon(4S)$ decays when prompt leptons from semileptonic decays of neutral B mesons are selected. With the assumption of CPT invariance, the flavor and mass eigenstates of the neutral B mesons are related by

$$\begin{aligned} |B_H\rangle &= p|B^0\rangle + q|\bar{B}^0\rangle, \\ |B_L\rangle &= p|B^0\rangle - q|\bar{B}^0\rangle, \end{aligned} \quad (1)$$

where $|p|^2 + |q|^2 = 1$. The time-dependent decay rate for same-sign dileptons is given by

$$\Gamma_{\Upsilon(4S) \rightarrow \ell^+ \ell^+}(\Delta t) = \frac{|A_\ell|^4}{8\tau_{B^0}} e^{-|\Delta t|/\tau_{B^0}} \left| \frac{p}{q} \right|^2 \left[\cosh\left(\frac{\Delta\Gamma}{2}\Delta t\right) - \cos(\Delta m_d \Delta t) \right] \quad (2)$$

for the $\ell^+ \ell^+$ sample. For the $\ell^- \ell^-$ sample, p/q is replaced by q/p . Here Δm_d and $\Delta\Gamma$ are the differences in mass and decay width between the two mass eigenstates, τ_{B^0} is the average lifetime of the two mass eigenstates, and Δt is the proper time difference between the two B meson decays. In this analysis only the absolute value of Δt is used. It is assumed that the semileptonic decay of the neutral B meson is flavor specific and CP conserving, so that $A_\ell = \bar{A}_\ell$, where $A_\ell \equiv \langle X^- \ell^+ \nu_\ell | B^0 \rangle$ and $\bar{A}_\ell \equiv \langle X^+ \ell^- \bar{\nu}_\ell | \bar{B}^0 \rangle$. If CP is not conserved in mixing, the condition $|p/q| = 1$ is no longer true and the decay rates for $\ell^+ \ell^+$ and $\ell^- \ell^-$ samples can differ. As can be seen in Eq. 2, the Δt dependence is the same for the $\ell^+ \ell^+$ and $\ell^- \ell^-$ samples, and therefore the CP violation shows up as a Δt -independent charge asymmetry, defined as

$$A_{\text{sl}} \equiv \frac{\Gamma_{\Upsilon(4S) \rightarrow \ell^+ \ell^+} - \Gamma_{\Upsilon(4S) \rightarrow \ell^- \ell^-}}{\Gamma_{\Upsilon(4S) \rightarrow \ell^+ \ell^+} + \Gamma_{\Upsilon(4S) \rightarrow \ell^- \ell^-}} = \frac{1 - |q/p|^4}{1 + |q/p|^4} \simeq \frac{4\text{Re}(\epsilon_B)}{1 + |\epsilon_B|^2}. \quad (3)$$

Here ϵ_B corresponds to the ϵ_K describing CP violation in the neutral K meson system. Standard Model calculations give the size of this asymmetry to be of the order of 10^{-3} [2, 3]. A significantly larger value would therefore be an indication of new physics.

Experimentally, a measurement of same-sign dilepton events that originate from $B^0 \bar{B}^0$ and $\bar{B}^0 B^0$ initial states requires careful charge-dependent corrections, which are done in several steps. First, the contribution from continuum $e^+ e^- \rightarrow q \bar{q}$ (where $q = u, d, s$ or c) to same-sign dilepton events is subtracted using off-resonance data. Second, all detected lepton tracks are corrected for charge asymmetries in the efficiencies for track finding and lepton identification, and for the probabilities of misidentifying hadrons as leptons. After these corrections, the remaining same-sign dilepton events still contain backgrounds from $B^0 \bar{B}^0$ and $B^+ B^-$ events. The last step of this analysis is to separate the signal events from these background events using their different behavior in the Δt distributions.

II. BELLE DETECTOR

This analysis is based on a data sample of 78 fb^{-1} at the $\Upsilon(4S)$ resonance (“on-resonance”) and 9 fb^{-1} at 60 MeV below the $\Upsilon(4S)$ resonance (“off-resonance”) collected

with the Belle detector [4] at the KEKB asymmetric e^+e^- collider [5]. The Belle detector is a large-solid-angle magnetic spectrometer that consists of a three-layer silicon vertex detector (SVD), a 50-layer central drift chamber (CDC) for tracking, a mosaic of aerogel threshold Cherenkov counters, time-of-flight scintillation counters (TOF), and an array of CsI(Tl) crystals for electromagnetic calorimetry (ECL) located inside of a superconducting solenoid coil that provides a 1.5 T magnetic field. An iron flux-return located outside of the coil is instrumented to detect K_L^0 mesons and to identify muons (KLM).

A. Track Finding Efficiency

The track finding efficiency is determined by analyzing a sample where simulated single electron or muon tracks are overlaid on hadronic events taken from experimental data. Lepton tracks are generated to cover the region of $1.2 \text{ GeV}/c < p^* < 2.3 \text{ GeV}/c$ and $30^\circ < \theta_{\text{lab}} < 135^\circ$, where p^* is the lepton momentum in the e^+e^- center-of-mass (c.m.) frame and θ_{lab} is the angle of the lepton track with respect to the z -axis in the laboratory frame. The z -axis passes through the nominal interaction point, and is anti-parallel to the positron beam direction. The track finding efficiencies are obtained for each bin of p^* (1.2–1.3, 1.3–1.4, 1.4–1.5, 1.5–1.6, 1.6–1.8, 1.8–2.0 and 2.0–2.3 GeV/ c), and θ_{lab} (30° – 37° , 37° – 50° , 50° – 77° , 77° – 82° , 82° – 111° , 111° – 119° , 119° – 128° and 128° – 135°). Figure 1 shows θ_{lab} -averaged track finding efficiencies for positive and negative tracks separately and their fractional differences as functions of p^* for electron and muon tracks. Events in all θ_{lab} regions are combined in these plots. The charge dependence of the track finding efficiency for both electrons and muons is less than 1.0%.

B. Lepton Identification

The most important contribution to the electron identification comes from examination of the ratio of the ECL cluster energy to the track momentum measured in the CDC. This information is combined with the shower measurement in the ECL, the specific ionization measurements (dE/dx) in the CDC, matching information between the ECL cluster position and extrapolated position of the CDC track, and the ACC light yield to form an electron likelihood \mathcal{L}_e [6].

The two-photon process $e^+e^- \rightarrow (e^+e^-)e^+e^-$ is used to estimate the electron identification efficiency. For this data sample, events are required to have: i) two tracks with particle identification information inconsistent with a muon hypothesis, laboratory momenta greater than 0.5 GeV/ c and transverse momenta greater than 0.25 GeV/ c ; ii) at least one ECL cluster with energy greater than 20 MeV. The two tracks are required to have: i) an acolinearity angle whose cosine is greater than -0.997 ; ii) a transverse-momentum sum less than 0.2 GeV/ c ; iii) a longitudinal momentum sum of less than 2.5 GeV/ c in the c.m. frame; iv) an invariant mass less than 5 GeV/ c^2 . In addition, the sum of the ECL cluster energies has to be between 0.6 GeV and 6.0 GeV. The electron identification efficiency is obtained by taking the ratio of the number of tracks selected with the above requirements with and without additional electron identification requirements.

For muon identification, CDC tracks are extrapolated to the KLM and the measured range and transverse deviation in the KLM is compared with the expected values to form a muon likelihood \mathcal{L}_μ [7]. The muon identification efficiency is determined by analyzing a

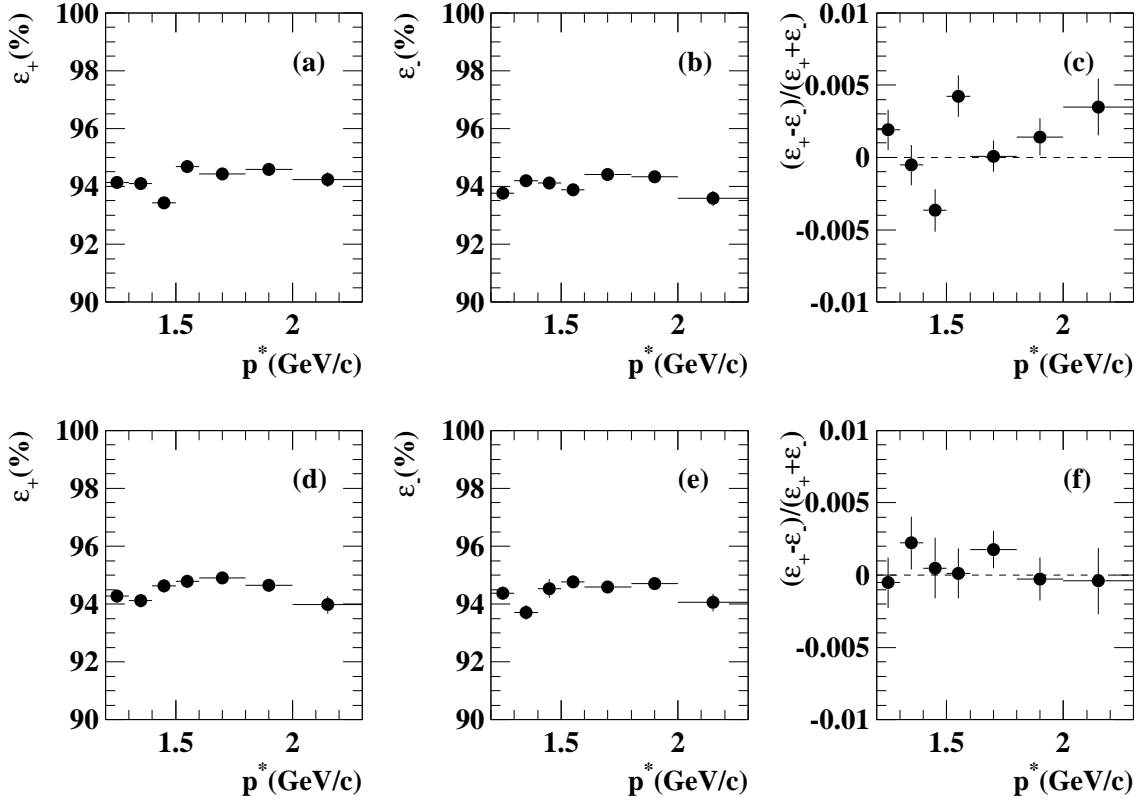


FIG. 1: θ_{lab} -averated track finding efficiencies as a function of c.m. momentum for positron tracks ϵ_+ (a), electron tracks ϵ_- (b), and charge dependence defined as $(\epsilon_+ - \epsilon_-)/(\epsilon_+ + \epsilon_-)$ (c). Corresponding plots for muon tracks are shown in (d), (e), and (f)

data sample where simulated single-muon tracks are overlaid on the hadronic events taken from experimental data.

The lepton identification efficiencies are obtained in the same p^* and θ_{lab} bins used for the track finding efficiency study. Figure 2 shows the θ_{lab} -averaged charge-dependent lepton identification efficiencies, where electron tracks are required to satisfy $\mathcal{L}_e > 0.8$, and the muon tracks are required to satisfy $\mathcal{L}_\mu > 0.9$ and to have a reduced χ^2 value for their transverse deviations in the KLM of less than 3.5. The charge dependence of the identification efficiency is less than 1% for both electrons and muons. Exactly the same criteria are imposed to select signal leptons.

C. Hadron Misidentification

The information on the ACC light yield, the time-of-flight measurement, and dE/dx measurements in the CDC is combined to provide hadron likelihoods: \mathcal{L}_π for pions, \mathcal{L}_K for

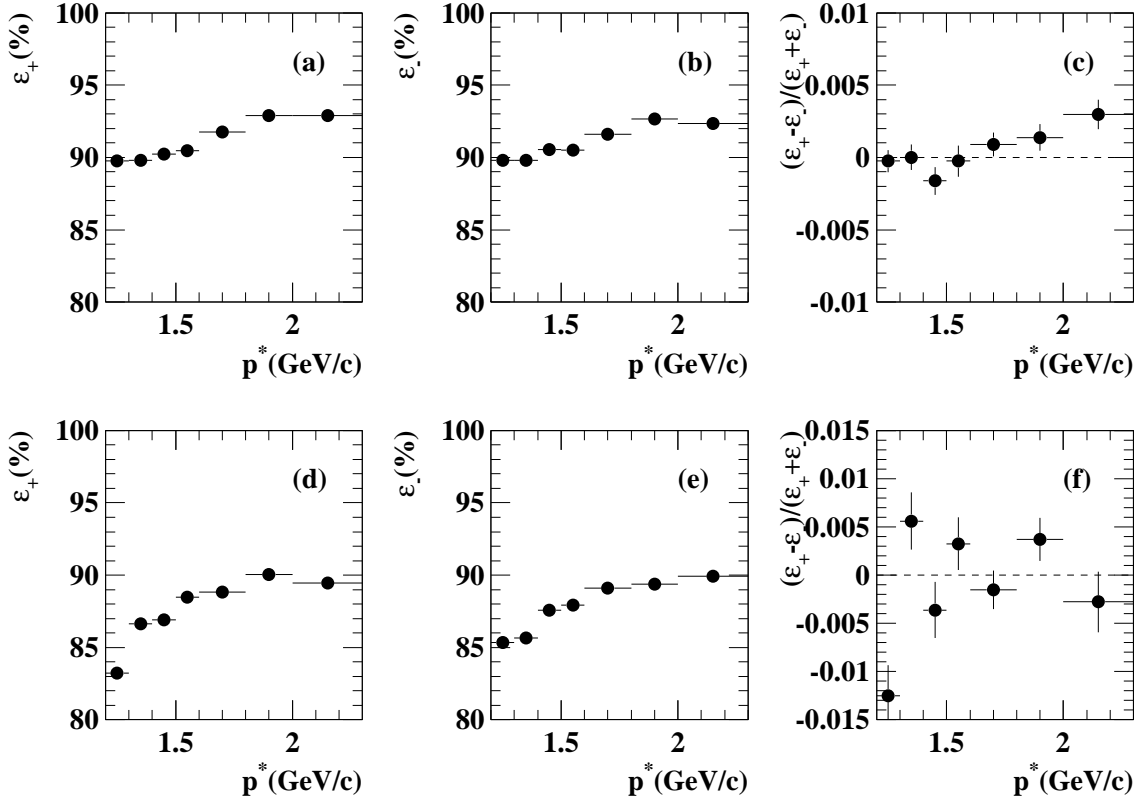


FIG. 2: The θ_{lab} -averaged identification efficiencies as a function of c.m. momentum for positrons ε_+ (a), electrons ε_- (b), and charge dependence defined as $(\varepsilon_+ - \varepsilon_-)/(\varepsilon_+ + \varepsilon_-)$ (c). Corresponding plots for muons are shown in (d), (e), and (f).

kaons, and \mathcal{L}_p for protons.

The hadron fake rate, which is defined as the probability that a hadron track is misidentified as a lepton, is determined from a sample of $K_S^0 \rightarrow \pi^+\pi^-$ decays for pions, $\phi \rightarrow K^+K^-$ decays for kaons, and $\Lambda \rightarrow p\pi^-$ ($\bar{\Lambda} \rightarrow \bar{p}\pi^+$) decays for protons. These decays are selected from a hadronic event sample described below. To select these track-pair combinations, the distance of closest approach with respect to the run-dependent interaction point and the position of the decay vertex are used. The difference in z position of the two tracks and the angle between position vector of the decay vertex and the momentum vector of K_S^0 or $\Lambda(\bar{\Lambda})$ in r - ϕ plane at the decay vertex are also used. When evaluating the fake rate for positively charged tracks, invariant masses are plotted for a sample of pairs where both tracks satisfy the above criteria and the negative track satisfies an additional hadron identification requirement. The signal yields are obtained by fitting the resulting mass distribution to a sum of a double Gaussian signal and a smooth background function in two ways: once without imposing any lepton identification requirement and once after imposing the lepton identification requirement on the positive track. The ratio of the two signal yields gives the fake rate for the positive charged tracks. The following requirements are imposed

on the likelihood ratios: $\mathcal{L}_\pi/(\mathcal{L}_\pi + \mathcal{L}_K) > 0.8$ for pions in $K_S^0 \rightarrow \pi^+\pi^-$, $\mathcal{L}_K/(\mathcal{L}_K + \mathcal{L}_\pi) > 0.8$ for kaons in $\phi \rightarrow K^+K^-$, and $\mathcal{L}_\pi/(\mathcal{L}_\pi + \mathcal{L}_p) > 0.8$ for pions in $\Lambda \rightarrow p\pi^-$. The fake rate for negatively charged tracks is obtained by repeating the procedure above with the roles of negative and positive tracks reversed.

In this study, because of low statistics, θ_{lab} -averaged values are used, and some p^* bins are combined.

Figure 3 shows the hadron fake rates as a function of momentum in the laboratory frame. The rate of pions faking electrons is at most 0.1% for both charges. The rate of kaons faking electrons decreases rapidly as p_{lab} becomes larger and is less than 0.2% for $p_{\text{lab}} > 1.4$ GeV/ c , with no significant charge dependence. While the rate of protons faking positrons is nearly zero, the rate for anti-protons faking electrons is as large as 4% due to the large anti-proton annihilation cross section in the ECL. Because of low statistics, the rate of protons faking positrons is obtained from the θ_{lab} -averaged value over all momenta. The rate of pions faking muons is about 1% for $p_{\text{lab}} > 1.5$ GeV/ c and shows no significant charge dependence. The rate of kaons faking muons is 1% to 2%, with that for K^+ being about 50% larger than that for K^- due to the larger kaon-nucleon cross section for the K^- . The rate of protons faking muons is less than 0.4% and shows no clear charge dependence.

III. EVENT SELECTION

A. Hadronic Event Selection

Hadronic events are required to have at least five tracks, an event vertex with radial and z coordinates within 1.5 cm and 3.5 cm, respectively, of the nominal beam interaction point, a total reconstructed c.m. energy greater than 0.5 W (W is the c.m. energy), a net reconstructed c.m. momentum with a z component less than 0.3 W/c , a total energy deposited in the ECL between 0.025 and 0.9 W , and a ratio R_2 of the second and zeroth Fox-Wolfram moments [8] of less than 0.7.

B. Dilepton Event Selection

Lepton candidates are selected from among the charged tracks by requiring the criteria previously described. In both electron and muon cases, a distance of closest approach to the run-dependent interaction point less than 0.05 cm radially and 2.0 cm in z is required. At least one SVD hit per track in the r - ϕ view and two SVD hits in the r - z view are required. To eliminate electrons from $\gamma \rightarrow e^+e^-$ conversions, electron candidates are paired with all other oppositely charged tracks and the invariant mass (assuming the electron mass) $M_{e^+e^-}$ is calculated. If $M_{e^+e^-} < 100$ MeV/ c^2 , the electron candidate is rejected. If a hadronic event contains more than two lepton candidates, the two with the highest c.m. momenta are used.

The two lepton candidates must satisfy additional criteria. The c.m. momentum of each lepton is required to be in the range 1.2 GeV/ $c < p^* < 2.3$ GeV/ c . The lower threshold reduces contributions from secondary charm decay; the upper threshold reduces continuum contributions. Each lepton track must be in the range $30^\circ < \theta_{\text{lab}} < 135^\circ$, where it has better z vertex resolution and lepton identification. Events that contain one or more J/ψ candidates are rejected. The invariant mass of each candidate lepton paired with each oppositely charged track (assuming the corresponding lepton mass) is calculated. If the invariant mass

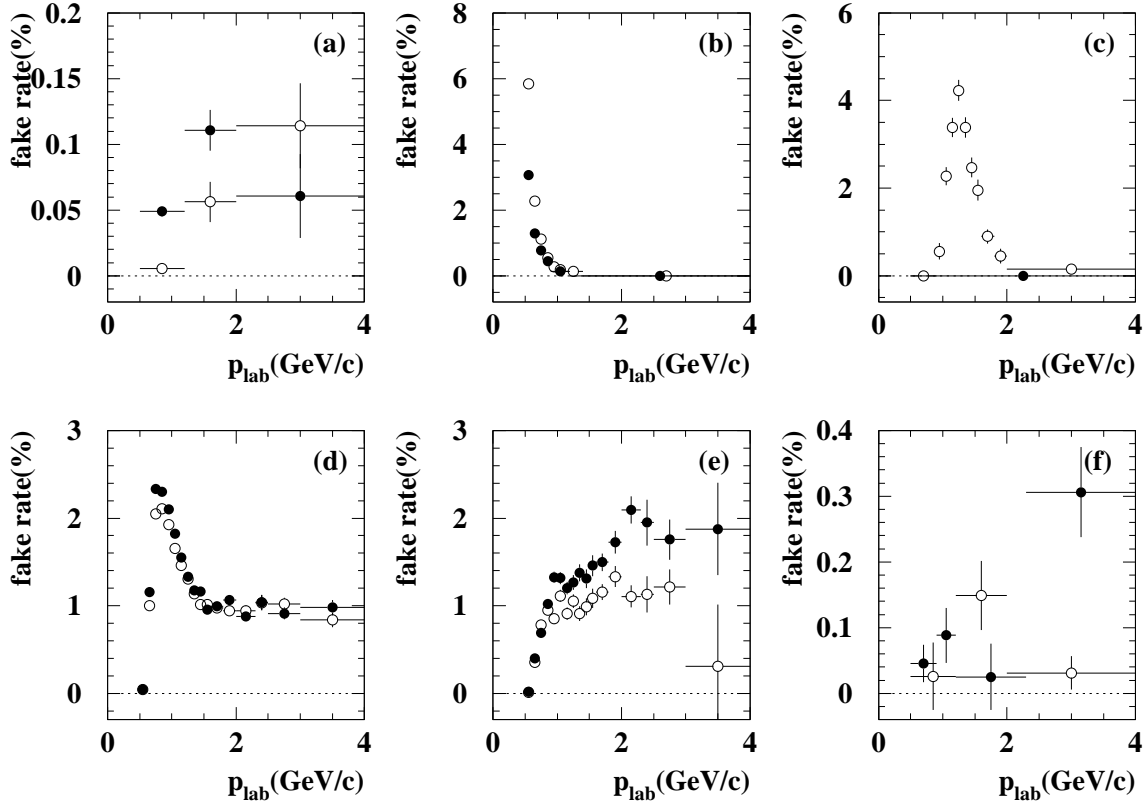


FIG. 3: Rates of pions ((a) and (d)), kaons ((b) and (e)), and protons ((c) and (f)) faking electrons and muons vs. laboratory momentum. Filled circles are for positive tracks and open circles are for negative tracks. The increase in the rate of kaons faking electrons at low momentum clearly visible in (b) is due to the overlap of the electron and kaon energy-loss bands; the other distributions are discussed in the text. Note that the minimum values of vertical axes are set to negative values. The dotted lines shows fake rate equal to zero.

falls within the J/ψ region, defined as $-0.15 \text{ GeV}/c^2 < (M_{e^+e^-} - M_{J/\psi}) < 0.05 \text{ GeV}/c^2$ or $-0.05 \text{ GeV}/c^2 < (M_{\mu^+\mu^-} - M_{J/\psi}) < 0.05 \text{ GeV}/c^2$, the candidate event is rejected. The looser lower mass window for the electron pair invariant mass accomodates bremsstrahlung of the daughter electron(s).

As can be seen in Figure 4, distributions of the opening angle of the two tracks in the c.m. frame, $\cos \theta_{\ell\ell}^*$, for the $\mu\mu$ and $e\mu$ pairs show distinct peaks in the back-to-back direction ($\cos \theta_{\ell\ell}^* \simeq -1$). This background is caused by hadron tracks misidentified as muons among jet-like continuum events. Also, spikes can be seen at $\cos \theta_{\ell\ell}^* = 1$ for the $\mu\mu$ pair events. This structure is caused by jet-like continuum events where a non-muon track is identified as a muon because hits in the KLM from a nearby true muon are assigned to it. The dilepton opening angle in the c.m. frame $\theta_{\ell\ell}^*$ is required to satisfy $-0.80 < \cos \theta_{\ell\ell}^* < 0.95$ in order to reduce this background.

With these selection criteria there are 46533 positive and 45477 negative same sign

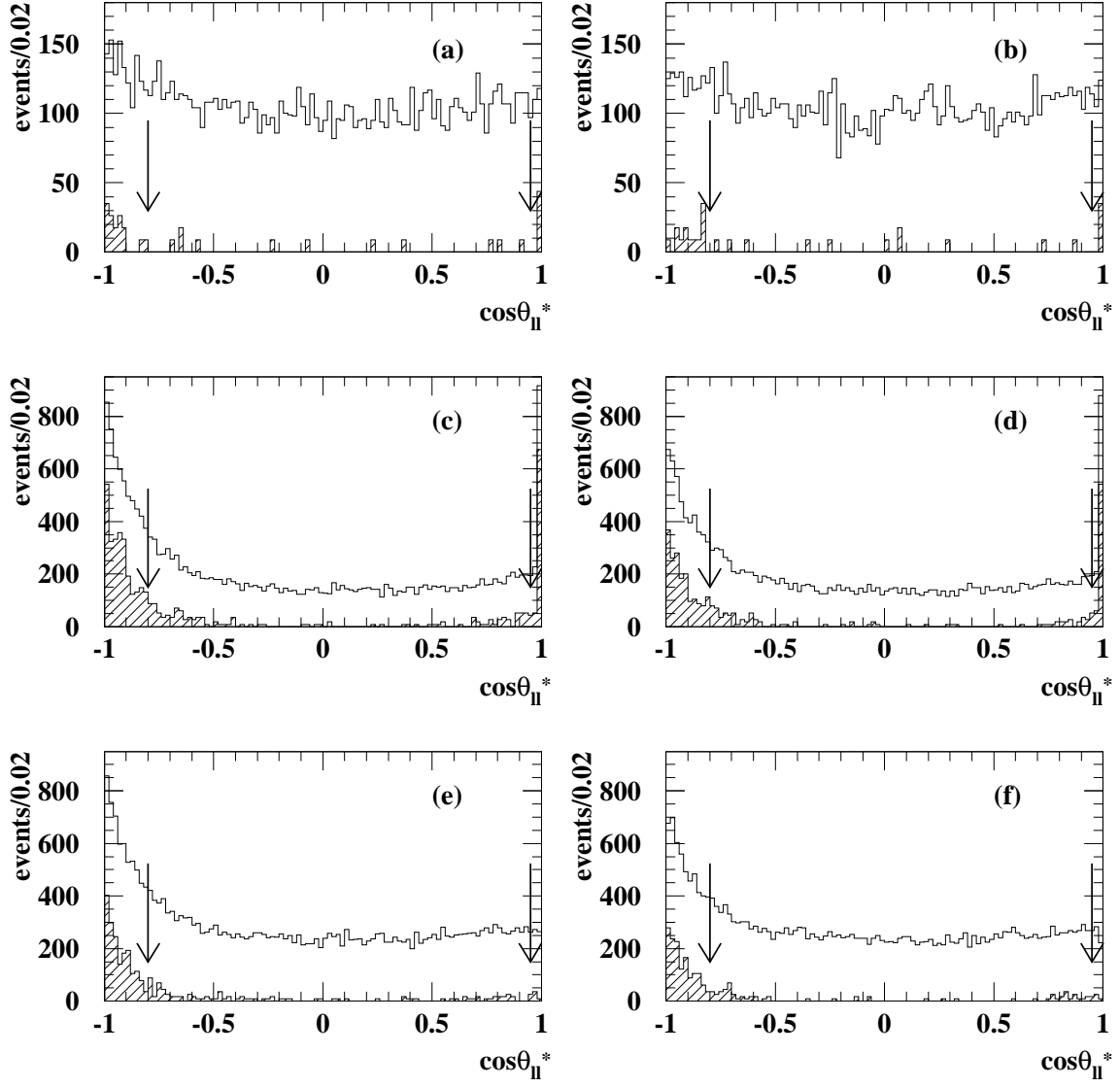


FIG. 4: $\cos\theta_{\ell\ell}^*$ distributions for dilepton samples in the on-resonance (open histogram) and scaled off-resonance (filled histogram) data. (a),(b) show ee events, (c),(d) show $\mu\mu$ events and (e),(f) are from $e\mu$ combinations. (a),(c) and (e) are the $++$ charge case and (b), (d) and (f) are the $--$ charge case. The arrows indicate the selection requirements.

dilepton events found in the on-resonance data. Continuum contributions are estimated to be 2230 for positive and 1574 for negative same sign events, based on the yield from off-resonance data. To estimate the continuum contribution from off-resonance data, off-resonance yields were scaled by the integrated luminosities and cross-section ratio. The

scaling factor is defined by

$$f = \frac{\int \mathcal{L}_{\text{on}} dt s_{\text{off}}}{\int \mathcal{L}_{\text{off}} dt s_{\text{on}}}. \quad (4)$$

where $\int \mathcal{L}_{\text{on(off)}} dt$ and $s_{\text{on(off)}}$ are the integrated luminosities and the square of c.m. energies for on(off)-resonance, respectively.

These dilepton yields, decomposed into three lepton categories, are given in Table I.

TABLE I: Numbers of dilepton events.

Combination	On-resonance		Off-resonance		Continuum	
	positive	negative	positive	negative	positive	negative
ee	9059	9028	11	11	96.2 ± 28.9	96.2 ± 28.9
$\mu\mu$	14672	14014	144	100	1259.2 ± 104.9	874.4 ± 87.4
$e\mu$	22802	22435	100	69	874.4 ± 87.4	603.4 ± 72.6
total	46533	45477	255	180	2229.8 ± 139.6	1574.0 ± 117.3

C. Δz Determination

The z -coordinate of each B meson decay vertex is the production point of the daughter lepton, which is determined from the intersection of the lepton track with the run-dependent profile of the interaction point. The distance between the z -coordinates of the two leptons, $|\Delta z|$, is defined as $|\Delta z| = |z(\ell_1) - z(\ell_2)|$.

In order to estimate the effect of detector resolution in the Δz distribution, J/ψ decays to e^+e^- and $\mu^+\mu^-$ are used. In these events, the two tracks originate from the same point, so the measured Δz , after the background contribution is subtracted, yields the detector resolution. Candidate J/ψ mesons are selected using the same requirements used for dilepton events, except for the J/ψ veto. The J/ψ signal regions are defined as $3.00 \text{ GeV}/c^2 < M(e^+e^-) < 3.14 \text{ GeV}/c^2$ and $3.05 \text{ GeV}/c^2 < M(\mu^+\mu^-) < 3.14 \text{ GeV}/c^2$ and the sideband region as $3.18 \text{ GeV}/c^2 < M(\ell^+\ell^-) < 3.50 \text{ GeV}/c^2$ for both electrons and muons.

The invariant mass distributions of J/ψ candidates are fitted to a function given by

$$N(M) = h_0 e^{-\frac{(M-M_0)^2}{2S^2}} + h_1 e^{-\frac{(M-M_0)^2}{2\sigma_1^2}} + A(M-B)^2 + C. \quad (5)$$

Here, h_0 and h_1 are the normalizations of the two Gaussians used to describe the signal, M_0 is the Gaussian mean which is common to both Gaussians, and σ_0 and σ_1 are the standard deviations of the Gaussians. A parameter S , defined as $S = \sigma_0$ for $M \geq M_0$ and $S = \sigma_0 + \alpha(M - M_0)$ for $M < M_0$, is introduced to modify the lower mass tail of one of the Gaussians to take the effect of bremsstrahlung into account. A , B and C are the parameters of the background function. The Δz distribution of the sideband region is scaled to the background yield in the signal region and subtracted from the signal region Δz distribution.

The J/ψ mass distributions and the Δz distributions are shown in Figure 5. The RMS values of the Δz distributions are $193 \mu\text{m}$ for $J/\psi \rightarrow e^+e^-$, $177 \mu\text{m}$ for $J/\psi \rightarrow \mu^+\mu^-$, and $185 \mu\text{m}$ for the combined $J/\psi \rightarrow \ell^+\ell^-$ sample.

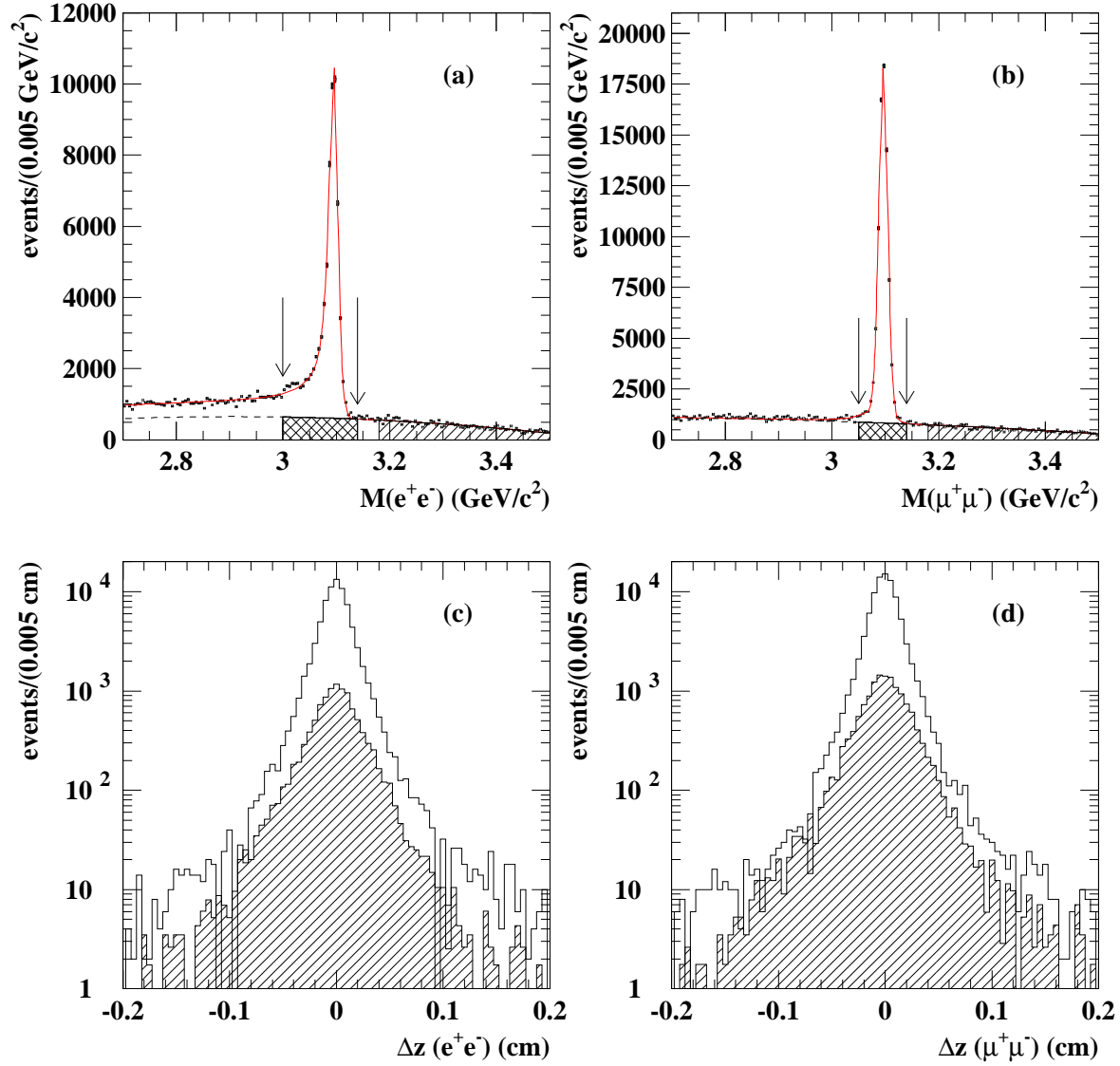


FIG. 5: Mass distributions for $J/\psi \rightarrow e^+e^-$ (a) and $J/\psi \rightarrow \mu^+\mu^-$ (b). The arrows indicate the selection criteria for each decay mode. The dashed lines indicate the fitted background component and the solid lines show the total fit results. The cross hatched area shows the estimated combinatorial background in the signal region and the single hatched area is the sideband region used to estimate the background Δz distribution. The Δz distributions for $J/\psi \rightarrow e^+e^-$ (c) and $J/\psi \rightarrow \mu^+\mu^-$ (d). Open histograms are for all J/ψ candidates in the signal region and hatched histograms are for the background.

D. Subtraction of Continuum Events

A sample of dilepton events originating from $B\bar{B}$ events is obtained by subtracting the luminosity and cross-section scaled off-resonance data from the on-resonance data. Since the kinematics of dilepton candidates in $B\bar{B}$ decays is different from those in continuum events in each of the variables $(p_1^*, p_2^*, \theta_1^*, \theta_2^*, \theta_{\ell\ell}^*, \Delta z)$, where $\theta_{1(2)}^*$ is the polar angle in the c.m. frame with respect to the beam axis of the more (less) energetic lepton, the subtraction should, in principle, be performed in this six-dimensional space, separately for each lepton flavor and charge combination.

Given the available statistics, this approach is not possible. Instead, we perform the subtraction by weighting the on-resonance and off-resonance yields for one of the six kinematical variables, while integrating over the five other variables. We obtain weighting factors for the six variables by repeating this procedure. Since, to a first approximation, the six variables are not correlated with each other, this approach provides the $B\bar{B}$ yield in the six variable space. The weighting factors are given by $w(k) = (1/r_{BB})(N_{\text{on}}(k) - fN_{\text{off}}(k))/N_{\text{on}}(k)$ where k denotes each of six variables, f is the scaling factor for the luminosity and c.m. energy introduced in Eq. 4, and $r_{BB} \equiv N_{B\bar{B}}^{\text{total}}/N_{\text{on}}^{\text{total}}$ is the fraction of total $B\bar{B}$ events in the on-resonance yield after integrating over all six variables; it is used for normalization. While the weighting factors show very little dependence on p_1^*, p_2^*, θ_1^* , and θ_2^* for all combinations of lepton flavors and charges, a clear dependence is observed for $\theta_{\ell\ell}^*$ in the case of the $\mu\mu$ and $e\mu$ data samples as shown in Figure 6. A clear dependence on Δz is also seen for all lepton pair combinations.

Using this method, the dilepton candidate yield for each lepton flavor and charge combination is then given in terms of the on-resonance yield and the weighting factors by

$$N_{B\bar{B}}(p_1^*, p_2^*, \theta_1^*, \theta_2^*, \theta_{\ell\ell}^*, \Delta z) = r_{BB} \prod_k w(k) N_{\text{on}}(p_1^*, p_2^*, \theta_1^*, \theta_2^*, \theta_{\ell\ell}^*, \Delta z). \quad (6)$$

The Δz distributions of the dilepton yields are obtained by projecting $N_{B\bar{B}}(p_1^*, p_2^*, \theta_1^*, \theta_2^*, \theta_{\ell\ell}^*, \Delta z)$ onto the $|\Delta z|$ axis.

IV. RESULT

A. Corrections to Lepton Candidates

The number of detected leptons for each lepton flavor and charge N_{det}^\pm is related to the number of true leptons N_ℓ^\pm by

$$N_{\text{det}}^\pm(p^*, \theta_{\text{lab}}) = N_\ell^\pm(p^*, \theta_{\text{lab}}) \varepsilon_{\text{trk}}^\pm(p^*, \theta_{\text{lab}}) \left\{ \varepsilon_{\text{pid}}^\pm(p^*, \theta_{\text{lab}}) + \sum_{h=\pi, K, p} r_{h\ell}^\pm(p^*, \theta_{\text{lab}}) \eta_{h\ell}^\pm(p^*, \theta_{\text{lab}}) \right\}, \quad (7)$$

where $\varepsilon_{\text{trk}}^\pm$ and $\varepsilon_{\text{pid}}^\pm$ are the efficiencies for track finding and lepton identification, $r_{h\ell}^\pm$ is the relative multiplicity of hadron of type h with respect to leptons of type ℓ in $B\bar{B}$ event, and $\eta_{h\ell}^\pm$ is the rate of hadrons h faking leptons ℓ . The relative multiplicities are determined from $B\bar{B}$ Monte Carlo (MC) events, and are shown in Figure 7. The relative multiplicities include the effects of decay-in-flight and interaction with the detector.

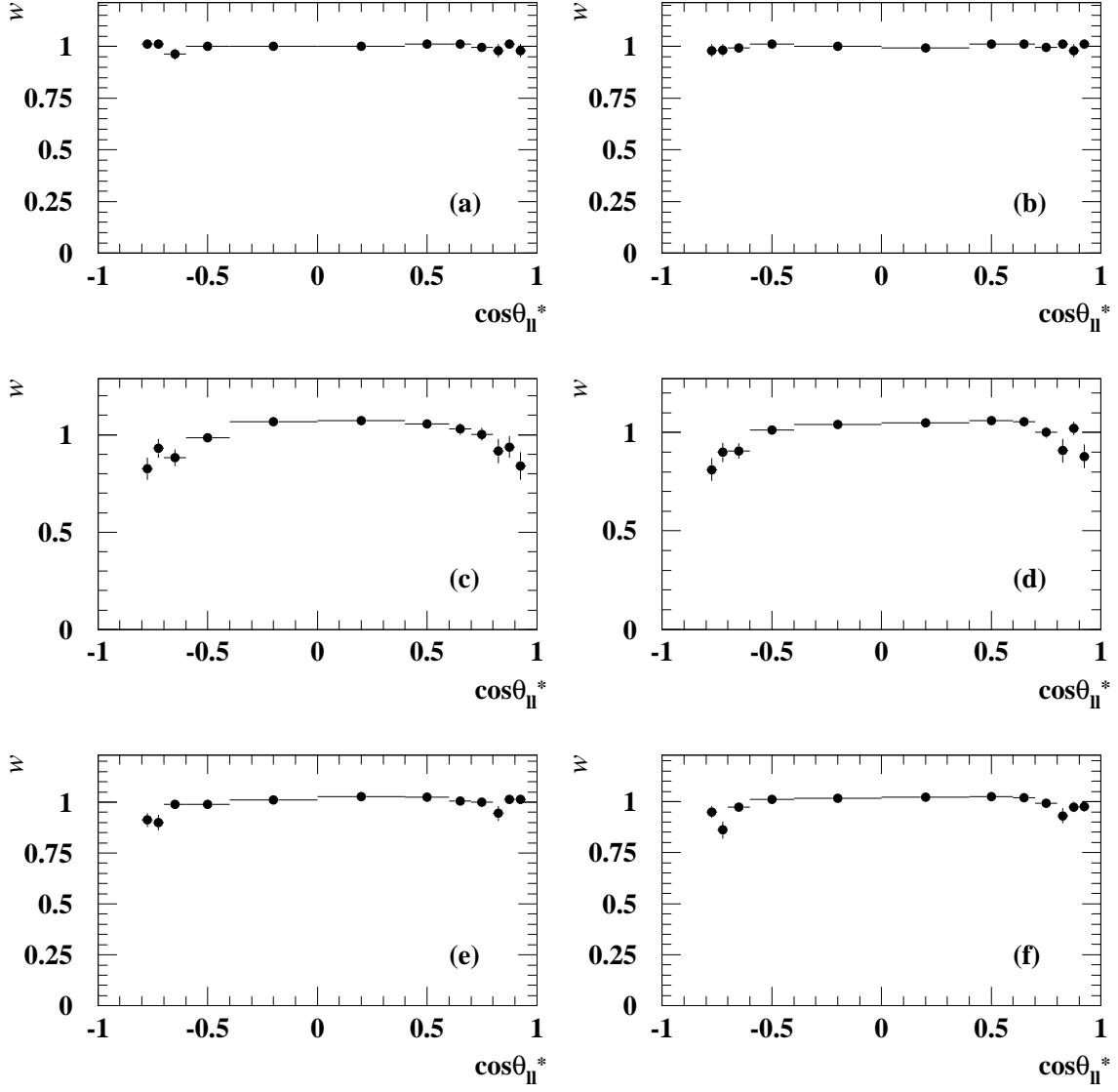


FIG. 6: $\cos\theta_{\ell\ell}^*$ dependence of the weighting factor for the fraction of the dilepton yield originating from $B\bar{B}$ decays in the on-resonance data for e^+e^+ (a) and e^-e^- (b) and corresponding quantities for $\mu\mu$ (c) and (d) and $e\mu$ (e) and (f).

Using the measured efficiencies, fake rates and the MC-determined relative multiplicities, the correction factors N_{ℓ}/N_{det} are determined in 7 bins of p^* (1.2–1.3, 1.3–1.4, 1.4–1.5, 1.5–1.6, 1.6–1.8, 1.8–2.0 and 2.0–2.3 GeV/c), and 8 bins of θ_{lab} (30° – 37° , 37° – 50° , 50° – 77° , 77° – 82° , 82° – 111° , 111° – 119° , 119° – 128° and 128° – 135°). (The fake rates are measured in the laboratory frame, but are converted into p^* - and θ_{lab} -dependent measurements for this correction.)

After the correction, the dilepton sample contains true leptons that come either from

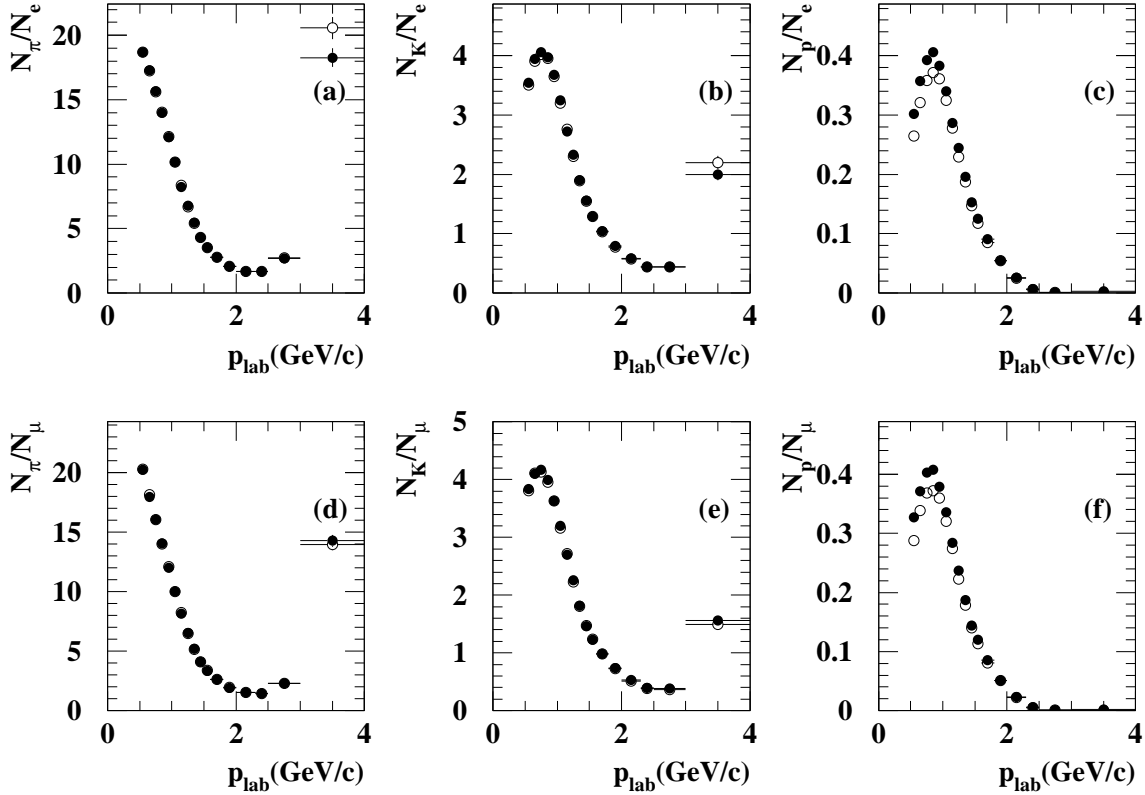


FIG. 7: Relative multiplicities of hadrons as a function of p_{lab} with respect to leptons. (a), (b) and (c) are for electrons and (d), (e) and (f) are for muons. (a) and (d) are pion to lepton, (b) and (e) are kaon to lepton, (c) and (f) are proton to lepton ratios. Filled circles are for positive tracks and open circles are for negative tracks. The effects of decay-in-flight and interaction with detector are included. Though in (a), (b), (d) and (e), the difference between positive and negative cases is less than 1%, in both (c) and (f), the proton rate is larger than the anti-proton rate by about 8%. The increases in multiplicities for pions and kaons around 3.5 GeV/c are due to two-body hadronic B decays.

prompt neutral B meson decay (signal) or from background processes such as charged B meson decay, secondary charm decay, or other leptonic B meson processes.

B. Fit to Δz Distribution

A binned maximum likelihood fit with signal and background contributions is used to extract $A_{\text{sl}}(|\Delta z|)$ from the Δz distribution. The overall background level is obtained from a fit with positive (++) and negative (--) samples combined. In this fit the Δz distribution for signal events is given by Eq. 2, assuming $\Delta\Gamma$ is small [9],

$$P^{\text{SS}} \propto e^{-|\Delta t|/\tau_{B^0}} (1 - \cos(\Delta m_d \Delta t)), \quad (8)$$

convolved with the detector response function described earlier. Here, τ_{B^0} and Δm_d are fixed to their world average values [9].

The backgrounds are divided into two categories: correctly tagged (*CT*), and wrongly tagged (*WT*). The *CT* category mainly contains events in which both leptons come from secondary charm decay in $B^0\bar{B}^0 \rightarrow B^0B^0(\bar{B}^0\bar{B}^0)$ (mixed) processes. The *WT* category contains events in which one lepton is from secondary charm decay of unmixed $B^0\bar{B}^0$ or B^+B^- and the other is from a semileptonic B decay. Though background Δz distributions are estimated using MC simulations, the MC underestimates the width of the Δz distribution. To correct for this, the MC Δz distribution is convolved with a Gaussian of standard deviation $\sigma = 69 \mu\text{m}$ [10]. The Δz distribution for the true same-sign dilepton events, where positive ($++$) and negative ($--$) samples are combined, is shown in Figure 8-(a) together with the fit results. The $\chi^2/n.d.f.$ of the fit is 48.75/38 (note that only statistical errors are included). In the fit, the ratio of *CT* to *WT* is fixed at the MC value, and only the ratio of signal and background is allowed to float. The MC-estimated *CT* and *WT* contributions to the Δz distribution are shown in Figure 8-(a).

C. Charge Asymmetry

The measured same-sign dilepton charge asymmetry is defined as

$$A_{\ell\ell}(\Delta z) = \frac{N^{++}(\Delta z) - N^{--}(\Delta z)}{N^{++}(\Delta z) + N^{--}(\Delta z)}, \quad (9)$$

where $N^{\pm\pm}(\Delta z)$ are the true dilepton yields as a function of Δz .

Since $N^{\pm\pm}(\Delta z)$ are the sum of signal and background, $N^{\pm\pm}(\Delta z) = N_s^{\pm\pm}(\Delta z) + N_b^{\pm\pm}(\Delta z)$, the dilepton charge asymmetry A_{sl} is related to $A_{\ell\ell}$ by

$$A_{\ell\ell}(\Delta z) = \frac{N_s^{++}(\Delta z) - N_s^{--}(\Delta z)}{N_s(\Delta z)} \frac{N_s(\Delta z)}{(N_s(\Delta z) + N_b(\Delta z))} = A_{\text{sl}}(\Delta z)d(\Delta z) \quad (10)$$

where $N_s = N_s^{++} + N_s^{--}$ and $N_b = N_b^{++} + N_b^{--}$. Here, $N_b^{++} = N_b^{--}$ is assumed. A dilution factor, $d(\Delta z) = N_s(\Delta z)/(N_s(\Delta z) + N_b(\Delta z))$, is calculated using the signal and background yields, which are determined in the fit given in Figure 8-(a). The result for $A_{\text{sl}}(\Delta z)$, determined from the measured $A_{\ell\ell}(\Delta z)$ and $d(\Delta z)$, is shown in Figure 9.

The dilepton charge asymmetry A_{sl} is a time integrated quantity and does not depend on Δz . Fitting this distribution to a constant in the region of $0.015 \text{ cm} < |\Delta z| < 0.200 \text{ cm}$, yields $A_{\text{sl}} = (-1.1 \pm 7.9) \times 10^{-3}$, with a $\chi^2/n.d.f.$ of 36.20/36 (again note that only statistical errors are included). The optimum fitting range is determined using a MC study that maximizes $N_s/\sqrt{N_s + N_b}$.

D. Cross Checks

As a consistency check, A_{sl} is obtained separately for the ee , $\mu\mu$, and $e\mu$ data samples. The results, $A_{\text{sl}}(ee) = (-13.3 \pm 14.4) \times 10^{-3}$, $A_{\text{sl}}(\mu\mu) = (+16.5 \pm 17.3) \times 10^{-3}$, and $A_{\text{sl}}(e\mu) = (-3.6 \pm 11.3) \times 10^{-3}$, are consistent with the primary result. Here the errors are statistical only.

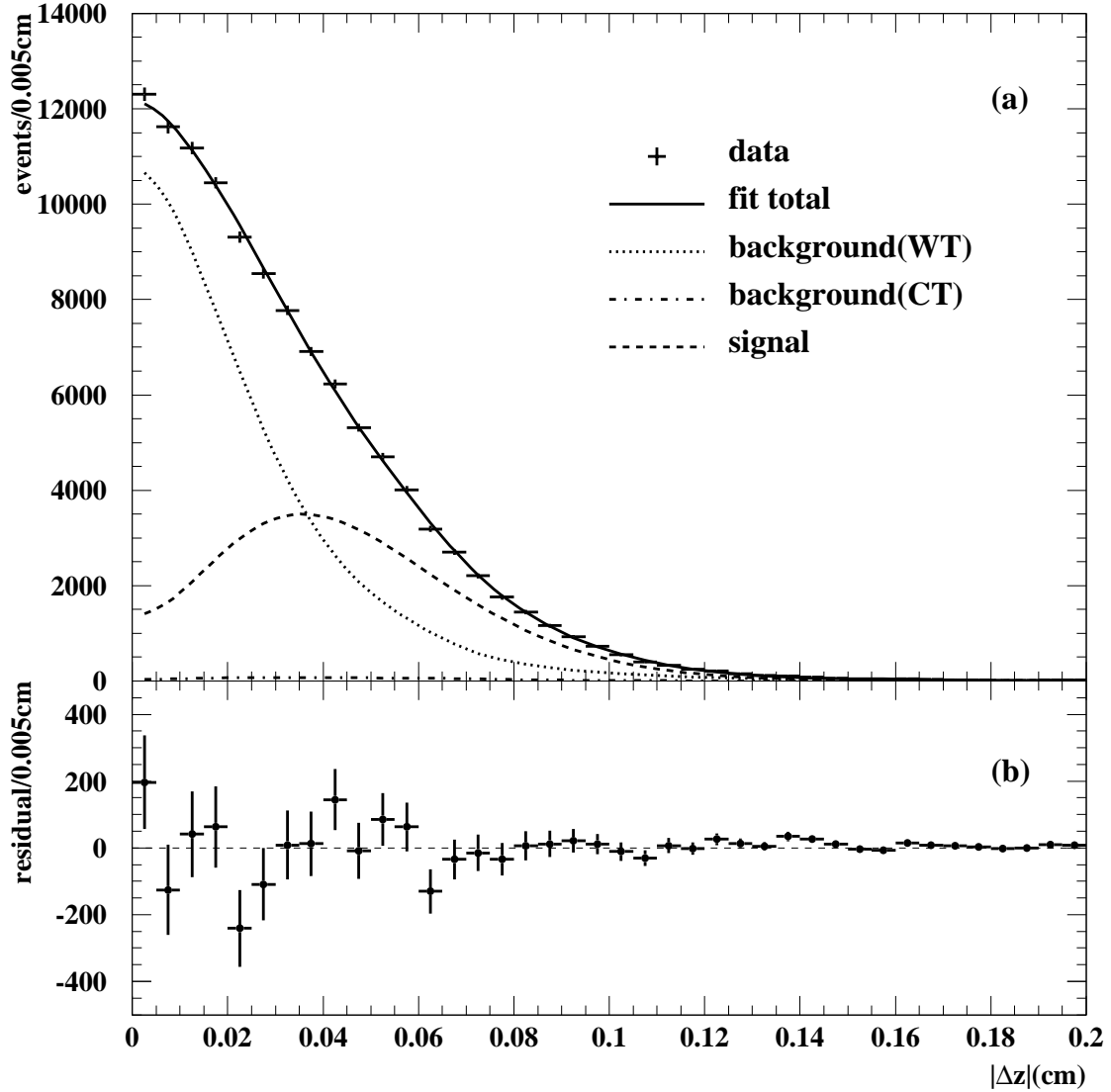


FIG. 8: (a) Δz distribution for the true dilepton events ($++$ and $--$ are combined). Points with error bars are data. The dot-dashed line shows the contribution from CT backgrounds, the dotted line shows the WT background contributions, the dashed line indicates the signal component and the solid line indicates the fitted total. (b) Difference between data and fit result as a function of $|\Delta z|$.

The validity of the assumption, to extract A_{sl} from $A_{\ell\ell}(\Delta z)$, is confirmed by repeating the fit without it. This yields $N_b^{++} = 20200 \pm 212$ and $N_b^{--} = 19766 \pm 210$ in the range $0.015 \text{ cm} < |\Delta z| < 0.200 \text{ cm}$, which is consistent with the initial assumption.

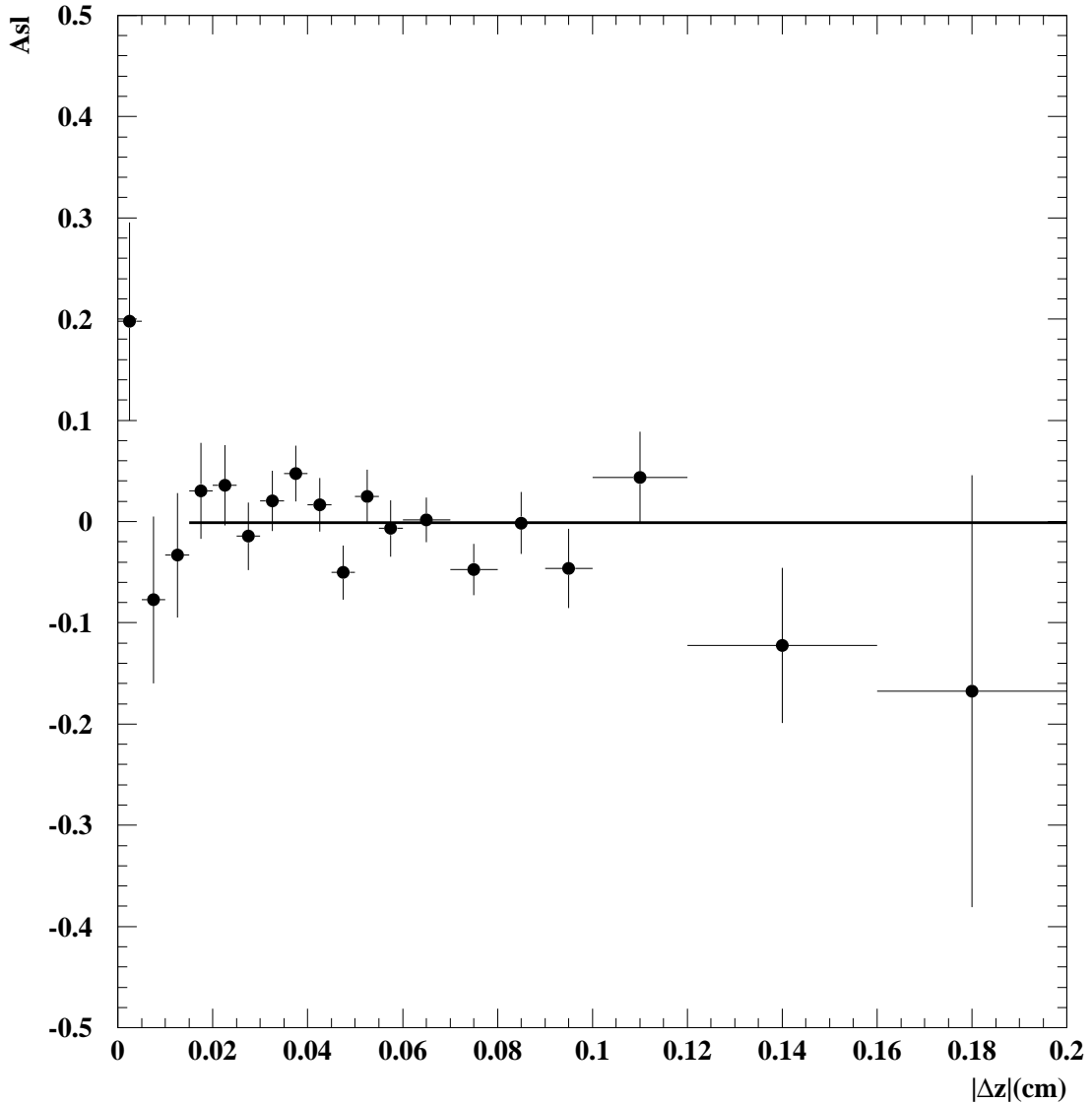


FIG. 9: $|\Delta z|$ distribution for A_{sl} .

E. Systematic Errors

Systematic errors in the determination of A_{sl} come from uncertainties in: i) the event selection criteria; ii) the continuum subtraction; iii) corrections for efficiencies of track finding and lepton identification and for lepton misidentification; iv) the dilution factor determination; and v) the Δz fit for the determination of A_{sl} .

Uncertainties in the selection criteria are estimated by repeating the analysis with different threshold values. For the track selection, the θ_{lab} lower (higher) limit is varied from the nominal 30° (135°) to 40° (125°) in ten (eighteen) steps, the closest-approach criterion in r - ϕ

from its nominal value of 0.05 cm to 0.02 cm in fourteen steps, the closest-approach criterion in r - z from 2 cm to 1 cm in fourteen steps, the p^* lower (higher) limit from its nominal value of 1.2 GeV/ c (2.3 GeV/ c) to 1.3 GeV/ c (2.2 GeV/ c) in fourteen steps, the requirement on the number of SVD hits by ± 1 from its nominal value of greater than or equal to two for r - z and one in r - ϕ . For the event selection, the $\cos\theta_{\ell\ell}^*$ lower (higher) criterion is varied from nominal -0.80 ($+0.95$) to -0.60 ($+0.70$) in twelve (seventeen) steps. In addition, the mass windows that reject J/ψ and $\gamma \rightarrow e^+e^-$ are widened by 20% and 50%, respectively.

To estimate the systematic error from the continuum subtraction, the analysis is repeated, varying the off-resonance yield by $\pm 1\sigma$.

For systematic uncertainties arising from the corrections to lepton candidates, we consider separately the effects due to the uncertainties in each bin and possible correlated sources of error. The fake rates from pions, kaons and protons and the lepton identification efficiencies are assumed to be independent. The systematic uncertainties from these track corrections are estimated by varying the efficiencies and fake rates by $\pm 1\sigma$ bin by bin. The systematic effects associated with the relative hadron multiplicities are estimated by varying the values by $\pm 1\sigma$ for all bins (both electron and muon) simultaneously. The uncertainties for each hadron species are estimated separately, assuming that the multiplicities of each are uncorrelated.

The contribution from the detector Δz response function is estimated by changing the response function shape according to the statistics of each Δz bin of $J/\psi \rightarrow \ell^+\ell^-$ sample. The contribution from the 69 μm smearing is estimated by repeating the analysis with 43 μm and 96 μm smearing, corresponding to the uncertainty in the difference of the resolution between data and MC. The contributions from uncertainties in Δm_d and τ_{B^0} are also estimated by varying the nominal values by $\pm 1\sigma$. The fitting range of the dilution factor determination is varied from its nominal range of $0.000 \text{ cm} < |\Delta z| < 0.200 \text{ cm}$ to $0.025 \text{ cm} < |\Delta z| < 0.200 \text{ cm}$. For the fitting range for the determination of the final A_{sl} , the lower limit is varied from 0.000 cm to 0.045 cm in nine steps. The results of the systematic error determination for A_{sl} are summarized in Table II.

V. CONCLUSION

The charge asymmetry for same-sign dilepton events from $\Upsilon(4S)$ decays has been measured. The result is related to the CP violation parameter in B^0 - \bar{B}^0 mixing,

$$A_{\text{sl}} = (-1.1 \pm 7.9(\text{stat}) \pm 7.0(\text{sys})) \times 10^{-3}, \quad (11)$$

or equivalently

$$|q/p| = 1.0005 \pm 0.0040(\text{stat}) \pm 0.0035(\text{sys}). \quad (12)$$

The measured A_{sl} is consistent with zero, or equivalently, $|q/p|$ is consistent with unity. This implies that CP violation in B^0 - \bar{B}^0 mixing is below the $O(10^{-2})$ level. The CP violation parameter ϵ_B can be calculated as

$$\frac{\text{Re}(\epsilon_B)}{1 + |\epsilon_B|^2} = (-0.3 \pm 2.0(\text{stat}) \pm 1.7(\text{sys})) \times 10^{-3}, \quad (13)$$

using the (exact) formula

$$\frac{\text{Re}(\epsilon_B)}{1 + |\epsilon_B|^2} = 0.5 \frac{1 - \sqrt{(1 - A_{\text{sl}})/(1 + A_{\text{sl}})}}{1 + \sqrt{(1 - A_{\text{sl}})/(1 + A_{\text{sl}})}}. \quad (14)$$

TABLE II: Source of systematic errors for the measurement of A_{sl} .

Category	Source	$\Delta A_{\text{sl}} (\times 10^{-3})$
Event selection	Track selection	± 2.61
	$\cos \theta_{\ell\ell}^*$ cut	± 0.63
	Lepton pair veto	± 2.33
Continuum subtraction		± 4.88
Track corrections	Track finding efficiency	± 1.56
	Electron identification efficiency	± 0.56
	Muon identification efficiency	± 1.98
	Fake electrons	± 0.45
	Fake muons	± 0.81
	Relative multiplicity	± 0.56
Δz fit for dileptons	Detector response function	± 0.07
	Δm_d	± 0.08
	τ_{B^0}	± 0.07
	69 μm smearing of background Δz	± 0.13
	Statistics of signal MC	± 0.01
	Statistics of background MC	± 0.19
	Fitting range	± 0.04
	Assuming $N_b^{++} = N_b^{--}$	± 1.59
Δz fit for A_{sl}	Fitting range	± 1.30
Total		± 6.97

These results are consistent with previous measurements [11] and provide significantly more restrictive bounds. Previous measurements of $\text{Re}(\epsilon_B)/(1 + |\epsilon_B|^2)$ are listed in Table III together with this measurement.

TABLE III: Comparison of the $\text{Re}(\epsilon_B)/(1 + |\epsilon_B|^2)$ measurements.

Experiment	$\text{Re}(\epsilon_B)/(1 + \epsilon_B ^2)$
ALEPH	-0.003 ± 0.007
CLEO	$0.0035 \pm 0.0103 \pm 0.0015$
BABAR	$(1.2 \pm 2.9 \pm 3.6) \times 10^{-3}$
This experiment	$(-0.3 \pm 2.0 \pm 1.7) \times 10^{-3}$

Acknowledgments

We thank the KEKB group for the excellent operation of the accelerator, the KEK cryogenics group for the efficient operation of the solenoid, and the KEK computer group

and the National Institute of Informatics for valuable computing and Super-SINET network support. We acknowledge support from the Ministry of Education, Culture, Sports, Science, and Technology of Japan and the Japan Society for the Promotion of Science; the Australian Research Council and the Australian Department of Education, Science and Training; the National Science Foundation of China under contract No. 10175071; the Department of Science and Technology of India; the BK21 program of the Ministry of Education of Korea and the CHEP SRC program of the Korea Science and Engineering Foundation; the Polish State Committee for Scientific Research under contract No. 2P03B 01324; the Ministry of Science and Technology of the Russian Federation; the Ministry of Higher Education, Science and Technology of the Republic of Slovenia; the Swiss National Science Foundation; the National Science Council and the Ministry of Education of Taiwan; and the U.S. Department of Energy.

-
- [1] A.B. Carter and A.I. Sanda, *Phys. Rev. Lett.* **45**, 952 (1980); *Phys. Rev.* **D23**, 1567 (1981).
 - [2] See, for example, A. Mohapatra, M. Satpathy, K. Abe, and Y. Sakai, *Phys. Rev.* **D58**, 036003 (1998), and references therein.
 - [3] R.N. Cahn and M.P. Worah, *Phys. Rev.* **D60**, 76006 (1999), Y. Nir, 27th SLAC Summer Institute on Particle Physics (1999), hep-ph/9911321, and references therein.
 - [4] Belle Collaboration, A. Abashian *et al.*, *Nucl. Instr. and Meth.* **A479**, 117 (2002).
 - [5] S. Kurokawa and E. Kikutani, *Nucl. Instrum. Meth.* **A499**, 1 (2003), and other papers included in this Volume.
 - [6] K. Hanagaki *et al.*, *Nucl. Instr. and Meth.* **A485**, 490 (2002).
 - [7] A. Abashian *et al.*, *Nucl. Instr. and Meth.* **A491**, 69 (2002).
 - [8] G.C. Fox and S. Wolfram, *Phys. Rev. Lett.* **41**, 1581 (1978).
 - [9] Particle Data Group, S. Eidelman *et al.*, *Phys. Lett.* **B592**, 1 (2004)
 - [10] Belle Collaboration, N. Hastings *et al.*, *Phys. Rev.* **D67** 052004 (2003).
 - [11] CDF Collaboration, F. Abe *et al.*, *Phys. Rev.* **D55**, 2546 (1996); OPAL Collaboration, G. Abbiendi *et al.*, *Eur. Phys. J.* **C12**, 609 (2000); ALEPH Collaboration, R. Barate *et al.*, *Eur. Phys. J.* **C20**, 431 (2001); CLEO Collaboration, D.E. Jaffe *et al.*, *Phys. Rev. Lett.* **86**, 5000 (2001); BABAR Collaboration, B. Aubert *et al.*, *Phys. Rev. Lett.* **88**, 231801 (2002).